Steering the Growth of Metal Ad-particles via Interface Interactions Between a MgO Thin Film and a Mo Support

Stefania Benedetti, Fernando Stavale, Sergio Valeri, Claudine Noguera, Hans-Joachim Freund, Jacek Goniakowski, and Niklas Nilius**

The coincidence lattice formed between a crystalline MgO film and a Mo(001) support is found to be an ideal template to produce long-range ordered ensembles of Fe and Cr particles for electronic, magnetic and chemical applications. The structural and electronic properties of this super-lattice are analyzed by means of scanning tunnelling microscopy and density functional theory. The different registers of atoms at the interface induce periodic changes in the MgO lattice parameter, in the metal-oxide binding length, and the workfunction. These variations modulate the adsorption landscape for Cr and Fe atoms and give rise to the observed ordering phenomena. Preferred nucleation and growth is revealed in those regions of the coincidence lattice that have a small lattice mismatch with the ad-particles and enable electron-transfer processes with the support.

1. Introduction

Nanostructured surfaces of high uniformity form the basis for various applications in optics, heterogeneous catalysis, gas-sensing and material sciences. Whereas powerful lithographic and imprinting techniques are available for patterning at the µm-scale, surface functionalization via self-assembly processes is commonly exploited in the nanometer regime. The self-ordering effects in the latter case are initiated by material deposition onto suitable template surfaces or by molecular superstructures that form as a result of adsorbate-adsorbate interactions.[1–3] While molecular-based overlayers usually lack the thermal and mechanical stability that is required for high temperature applications, robust templates can be fabricated out of metallic,[4,5] semiconducting,[6] and insulating materials.[7–9]

Traditional templates are surfaces with a small miscut from a low-index crystallographic plane and hence a regular sequence of step edges.[10–12] Alternatively, thin-film growth on a substrate with slightly different lattice parameter might be used, as the resulting misfit strain often triggers the development of a regular dislocation network.[4,7,8,13] These dislocation lines produce an inhomogeneous pattern of binding sites that can be decorated with suitable adsorbates and nanoparticles. Moreover, coincidence lattices due to structurally mismatched overlayers often introduce variations of several surface-electronic properties, such as workfunction, surface dipole and available state-density for hybridization.[14–16] The electronic modulations may be probed by suitable ad-species again that consequently become subject to self-ordering processes on the surface. By exploiting such patterning techniques, well-ordered superstructures consisting of single adatoms,[7,15] molecules,[1,11,17] and metal nanoparticles,[9,13,18] have been produced on macroscopic length scales.

In this work, we have explored the template effect induced by an MgO thin film grown on a Mo(001) support.[19] The 5% lattice mismatch between the respective bulk systems leads to the development of a square-shaped coincidence lattice of 55 Å-periodicity. Initiated by regular modulations of several MgO-Mo interface properties, the development of well-ordered ensembles of metal nanoparticles with small size-distribution is revealed in scanning tunnelling microscopy (STM) measurements. The thermodynamic incentives for the observed spatial organization are elucidated by density functional theory (DFT) calculations. Given its high temperature stability, the MgO/Mo template is particularly suited for the preparation of structurally uniform metal-particle ensembles for applications in heterogeneous catalysis.[20] The exceptionally small size-distribution of Cr and Fe particles would be beneficial also for the development of model systems for magnetic storage devices.

Dr. S. Benedetti, Prof. S. Valeri
Centro S3, Instituto Nanoscienze-CNR
and Dipartimento di Scienze Fisiche
Informatiche e Matematiche
Università di Modena e Reggio Emilia
via Campi 213/a, Modena, 41125, Italy
Dr. F. Stavale, Prof. H.-J. Freund, Dr. N. Nilius
Fritz-Haber-Institut der Max-Planck-Gesellschaft
Faradayweg 4-6, Berlin, 14195, Germany
E-mail: nilius@fhi-berlin.mpg.de
Prof. Claudine Noguera, Dr. J. Goniakowski
CNRS and Université Pierre et Marie Curie-Paris 6
INSP, UMR7588, 4 place Jussieu, Paris cedex 05, 75252, France
E-mail: jacek.goniakowski@insp.jussieu.fr

DOI: 10.1002/adfm.201201502

2. Results and Discussion

2.1. Coincidence Lattice

In this first section, we will summarize the experimental and theoretical characteristics of the misfit-induced MgO/Mo

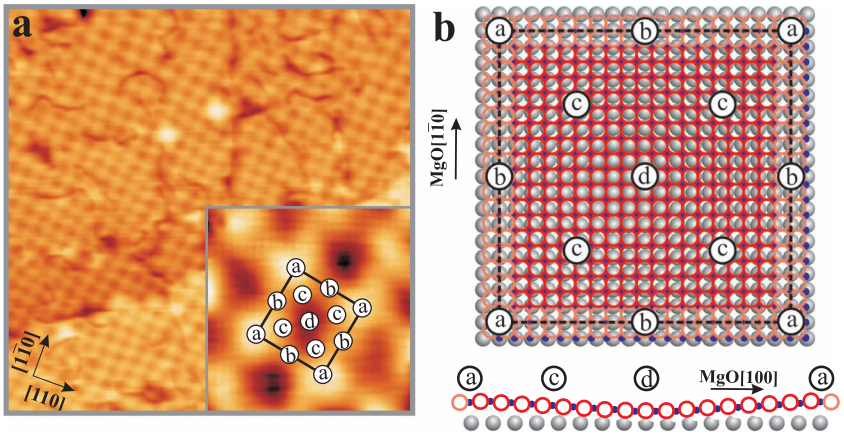

Figure 1. a) Topographic STM image of a 5 ML thick MgO/Mo(001) film showing the typical coincidence lattice (80 × 80 nm^2, 3.5V). The inset shows a close-up with the superstructure unit-cell and the main stacking regions marked with letters (12 × 12 nm^2). b) Ball model of the coincidence unit cell and vertical cut through of a monolayer MgO/Mo(001) film along the MgO[100] direction. Regions (a) and (d) denote the Mg-Mo and O-Mo domains, respectively, while (b) and (c) have intermediate stacking configurations.

coincidence lattice, while its impact on the nucleation behavior of metal particles is discussed in the subsequent paragraphs. The coincidence lattice becomes visible for MgO films of 1-7 ML thickness, when a square network of 55 Å-periodicity appears in the STM images (**Figure 1**a). The most elevated parts of the superstructure are the crossing points between the bright lines, which are imaged ≈1 Å above the dark squares in between. Employing X-ray diffraction measurements, the nature of the network has been identified as a coincidence lattice formed by 19 MgO unit cells overgrowing 18 cells of the Mo support.[21] Inside the super-lattice, regions of different interface registry are resolved, e.g., domains where either the Mg (Mg-Mo) or the O ions (O-Mo) of the oxide sit on top of the substrate Mo atoms. According to our DFT calculations, the O-Mo stacking is energetically favorable over the Mg-Mo configuration by 0.7 eV per interface atom. The attractive O-Mo interaction leads to a short interface distance of 2.3 Å in this region (**Figure 2**a), while the lateral Mg-O distance is enlarged by ≈5% with respect to bulk MgO in order to reach an epitaxial relationship with the Mo support (Figure 2b). Conversely, the lateral Mg-O distance contracts in the Mg-Mo domains, where an extra lattice plane that has no Mo counterpart is inserted into the MgO layer. The mainly repulsive Mg-Mo interaction in this region leads to an increased interface distance of 3.5 Å; a value that might be slightly overestimated due to the disregard of dispersive forces in our DFT approach. While in-plane modulations in the lattice parameter are most pronounced in the MgO interface layer, they remain detectable also in subsequent planes. With increasing film thickness, the region of minimal Mg-O bond lengths expands around the Mg-Mo domain and finally develops into a square-zone of 40 Å side length in the third MgO plane (Figure 2c). The out-of-plane lattice parameter is subject to periodic modulations as well, as it contracts in regions with long in-plane distances and expands in the others, following a tetragonal distortion of the MgO lattice (Figure 2b).

Electronically, the O-Mo stacking region is characterized by a negative workfunction change of $\Delta\varphi = -2.3$ eV with respect to bare Mo(001) (Figure 2a). It originates from the small metal-oxide interface separation in this domain, which suppresses the electron spill-out from the Mo support and removes the associated dipole and hence a main reason for the high workfunction of most metal surfaces. In contrast, the workfunction change is negligible in domains with Mg-Mo register ($\Delta\varphi = -0.3$ eV), as the large metal-oxide binding lengths in this configuration preserves the effect of electron spill-out. We note that the interface distance evolves monotonically in between these primary stacking regions, producing a substantial tilt of the oxide planes against the Mo(001) surface that in turn gives rise to distinct satellites in the diffraction data.[21] Following this geometric trend, also the workfunction decreases when going from Mg-Mo to O-Mo interface domains, as shown in Figure 2a.

On the basis of these results, regions of different STM contrast can be related to different stacking domains of the

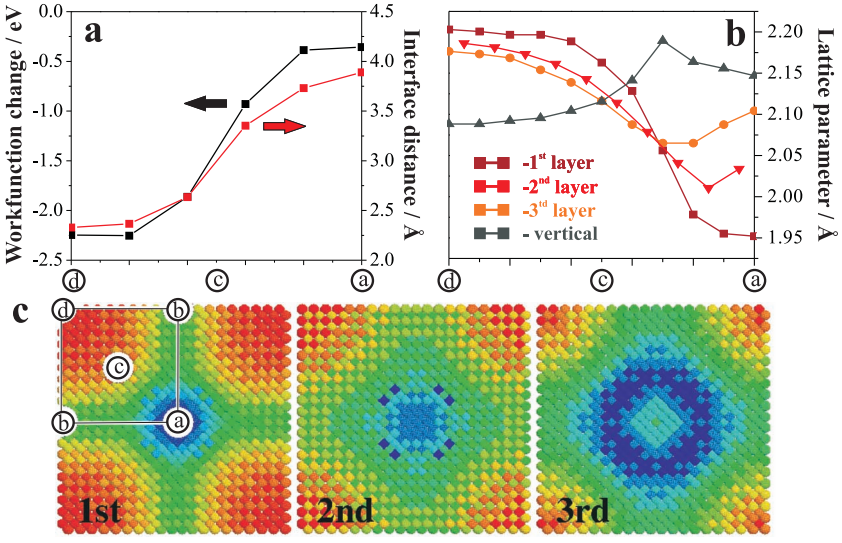

Figure 2. a) Interface separation and workfunction change with respect to clean Mo for six different interface registers of a 3 ML MgO/Mo(001) film, as obtained from DFT calculations. The regions are labelled according to the scheme in Figure 1. b) Structural distortion of the film calculated for the full MgO/Mo coincidence cell with a semiempirical approach.[22] The graph depicts the dependence of the in-plane lattice parameter of the first three MgO layers and the mean out-of-plane parameter on the interface register. c) Color-coded 2D maps of the in-plane parameter for the first three MgO planes. Long and short O-Mg distances are depicted with dark red and blue, respectively.

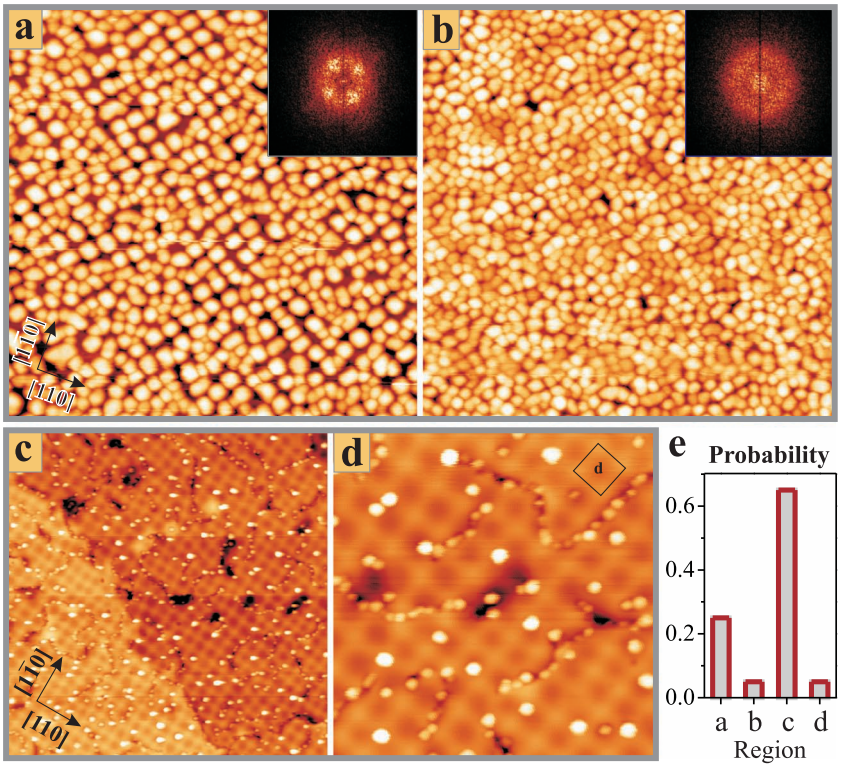

Figure 3. STM topographic images of 3 ML Fe deposited onto a) 5 ML and b) 15 ML MgO/Mo(001) films (100 × 100 nm^2, 3.5 V). The spatial ordering of the Fe particles in (a) becomes evident in the fast-Fourier transform shown in the inset. c) Overview (100 × 100 nm^2, 3.5 V) and d) close-up image (45 × 45 nm^2, 3.5 V) of 0.1 ML Cr dosed on a 5 ML thick MgO/Mo(001) film. A unit cell of the coincidence lattice is marked in the upper right. e) Histogram of Cr nucleation sites on the MgO/Mo coincidence lattice, as deduced from an analysis of around 500 aggregates.

coincidence lattice (Figure 1a). The Mg-Mo domains elevate by ≈1.0 Å above the O-Mo regions, suggesting an assignment of the former to the bright lines in the STM images. We further mention a relatively high density of point defects in the bright regions of the superstructure, in agreement with the energetically unfavorable situation of the Mg-Mo domains. Consequently, areas (a) and (d) in the experimental images shown in Figure 1 are assigned to regions with Mg-Mo and O-Mo register, respectively, while (b) and (c) denote two intermediate configurations. A more detailed discussion of the MgO/Mo coincidence lattice can be found in ref. [21,23].

2.2. Metal Deposition

The MgO/Mo coincidence lattice modulates not only several interface properties, but governs also the adsorption behavior, as seen for Fe and Cr deposition. Pronounced self-ordering effects become evident upon dosing 2–3 ML Fe onto a 5 ML thick MgO/Mo film (**Figure 3**a). The Fe particles organize themselves into a square lattice that mimics the periodicity of the coincidence cells in terms of inter-particle distance (55 Å) and particle density (3.6 × 10^{12} cm^{-1}*vs* 3.3 × 10^{12} cm^{-1} superstructure cells). Moreover, the deposits feature a rather narrow size distribution, characterized by a mean diameter of (30 ± 5) Å and a mean height of (15 ± 5) Å. Not surprisingly, the ordering effect depends on the film thickness. For 5–10 ML thick films, almost perfect long-range order is found, as the films are thin enough to render the adsorption sensitive to MgO/Mo interface phenomena but sufficiently thick to ensure high structural quality and low defect-concentration. Conversely, the ordering effect disappears above 20 ML film thickness, as the influence of the interface fades away (Figure 3b).

For Cr, even the nucleation sites inside the coincidence lattice have been identified, as smaller aggregates could be prepared and imaged as compared to Fe. After dosing 0.1 ML Cr, small deposits with bimodal size distribution were found on the surface. While particles of around 1.5 nm diameter nucleate along the MgO dislocation lines, 2.5 nm-wide deposits form on the oxide terraces (Figure 3c,d). Only the latter grow in size and density at higher metal exposure, while the defect-bound species exhibit self-limiting growth behavior. We tentatively ascribe the observed growth limitation to charging effects, in which the aggregates lose electrons to trap states inside the MgO dislocation lines.[24] This charge accumulation generates a repulsive Coulomb field around the deposits and hampers the attachment of further atoms, a phenomenon that is less pronounced on the stoichiometric terraces. While the position of the defect-bound aggregates is given by the course of the defect lines, the terrace-bound species are able to optimize their binding site within the MgO/Mo superstructure. As derived from dozens of STM images, Cr has a strong nucleation preference close to, but not on top of the bright maxima of the coincidence lattice, while the dark regions in between are avoided (Figure 3d). This binding peculiarity becomes even clearer in a histogram of nucleation sites, which shows that more than 65% of the Cr nuclei are actually located in region (c), i.e., in between the bright corner and the dark center of the coincidence cell (Figure 3e). The adjacent corner-regions (a) show considerable population as well, while the central part of the super-cells (d) is clearly disfavored. Assuming a Boltzmann distribution, we may estimate the difference in Cr adsorption energy between the most (c) and least favorable (d) binding region via: $n_c/n_d \propto \exp(-\Delta E/kT)$. The difference amounts to 65 meV for 300 K deposition temperature, but has to be considered as lower bound due to kinetic limitations in the nucleation process. In contrast to Fe, an irregular arrangement of differently sized particles develops at higher Cr exposure. The absence of spatial ordering in this case is explained with the presence of four, closely spaced nucleation sites in the super-cell, promoting coalescence of adjacent particles already at low Cr dose. The self-organization would be more likely if the preferred binding position would match a high-symmetry site of the coincidence lattice, such as a corner or a central position.

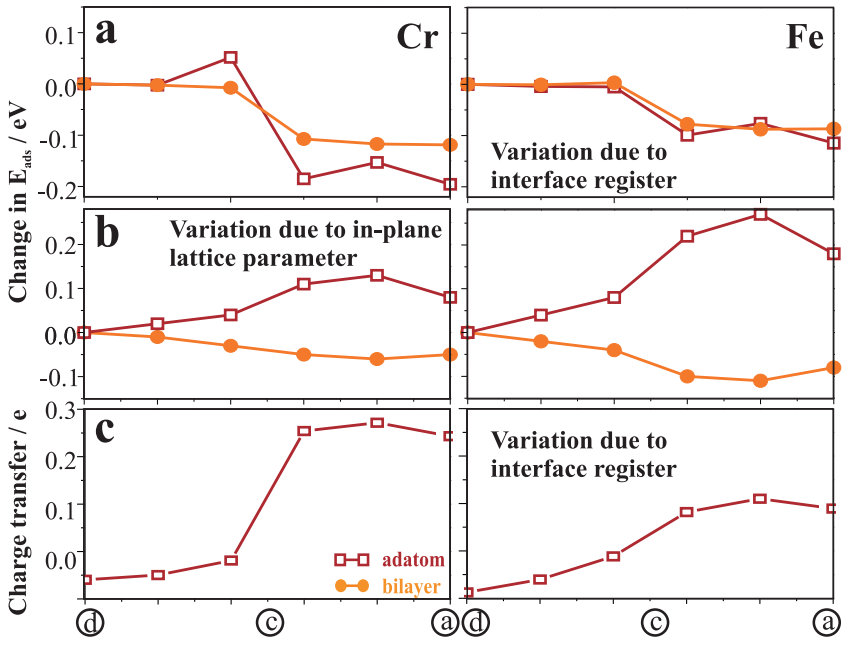

Figure 4. a,b) Relative binding energies (per atom) with respect to the O-Mo domain (region d) and c) charge transfer for Cr (Fe) adatoms and bilayers adsorbed on a 3 ML thick MgO/Mo(001) film shown as a function of interface register. Whereas data in (a) and (c) have been calculated with a constant in-plane lattice parameter, (b) displays the effect of the local lattice distortion induced by the Mo support.

2.3. Discussion

Taking advantage of our computational results, we will rationalize the observed site-specific nucleation of Cr and the spatial ordering of Fe on the MgO/Mo coincidence lattice in the following. A first ordering incentive comes from workfunction modulations as induced by changes in the interface registry. Single-atom adsorption is found to be strongest in the Mg-Mo domain, where the Cr and Fe binding strength is larger by 0.2 and 0.1 eV, respectively, as compared to the O-Mo region (**Figure 4**a,c). The Cr interaction in this region is characterized by a substantial electron transfer from the ad-species into the support, triggered by the high workfunction at Mg-Mo register. The charge exchange leads to a partial depopulation of the antibonding Cr $d_{z2\text{-}r2}$–O p_z orbital and enables electrostatic $Cr^{(+)}$–$O^{(-)}$ coupling, reinforcing the Cr-O bond (**Figure 5**). In contrast, the Cr remains neutral in O-Mo stacking regions, because the reduced workfunction inhibits the electron transfer. A similar trend is revealed for Fe, however the charge transfer into the Mg-Mo domains is weaker due to the higher electro-negativity of iron. We note that the energetic preference for an adsorption in the Mg-Mo domains persists at bilayer coverage of the ad-metal, although it is somewhat attenuated by the effect of metal-metal interactions.

A second effect comes from the local distortion of the MgO trilayer in presence of the Mo(001) support (Figure 2b). Its impact has been deduced from the adsorption of metal ad-species on a strained, unsupported MgO(001) trilayer. We find that an expansion of the in-plane lattice parameter, typical for the O-Mo domain, reinforces the adsorption of isolated adatoms (Figure 4b). The effect is relatively weak for Cr (≈0.1 eV) and hence unable to override the charge-transfer driven bond strengthening that is active in the Mg-Mo regions. For Fe atoms, on the other hand, the impact of the MgO distortion is larger (≈0.25 eV) and might overcome the stabilizing workfunction effect in the Mg-Mo domains. The trend becomes however reversed at higher metal coverage, as the simultaneous maximization of metal-metal and metal-substrate interactions promotes binding to regions with contracted in-plane lattice parameter (Figure 4b). This finding reflects the fact that the equilibrium interatomic distance in Fe and Cr dimers, clusters, films, and bulk crystals is systematically shorter than the in-plane lattice constant of the distorted MgO films. The observed preference for particle growth in the Mg-Mo domains is therefore a cooperative effect of workfunction and MgO lattice distortion.

Let us note that regions of contracted lattice parameter do not coincide with the very centers of the Mg-Mo domains, but rather expand into a square area around it. The size of this zone increases with film thickness and reaches around 40 Å in the third MgO layer (Figure 2c). The Fe deposits are now able to fill the entire zone of reduced lattice parameter, defining the size

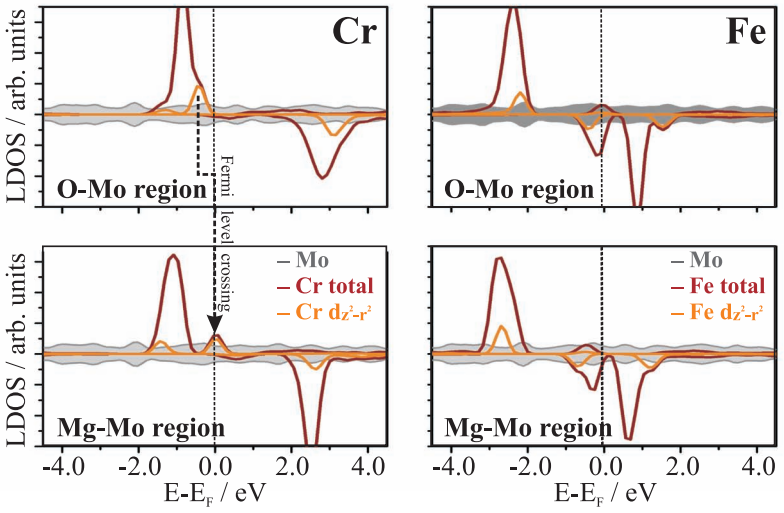

Figure 5. Projected, spin polarized density of states for Cr and Fe atoms bound to O-sites of a 3ML thick MgO/Mo(001) film for two interface registers. Note the partial depopulation of the Cr $d_{z2\text{-}r2}$-O p_z orbital for adsorption sites on the Mg-Mo interface domain.

of the ad-particles. Their lateral growth only stops when neighboring O-Mo domains are reached, that feature an increased interfacial lattice mismatch and do not support electron transfer into the substrate anymore. Both effects produce an energy barrier for the lateral expansion of the particles and rather promote their three-dimensional growth. The result is the observed narrow size-distribution of Fe deposits on the MgO/Mo films that is dictated by the favorable growth conditions in the Mg-Mo stacking domains. Also Cr tends to localize in regions with contracted lattice parameter, in agreement with the deduced nucleation preference in region (c) that is halfway between the Mg-Mo and O-Mo domains. In contrast to Fe, however, the growth of the Cr particles does not stop if zones of enlarged lattice parameter are reached, which causes the self-ordering effect to break down. One difference to Fe is a weaker lateral modulation of the Cr adsorption potential, which renders Cr nucleation possible even outside the preferred Mg-Mo domain. In addition, the total binding strength is reduced, which increases the diffusivity of the Cr adatoms and enhances the weight of Cr-Cr compared to Cr-MgO interactions.

3. Conclusions

The coincidence lattice formed between a MgO thin-film and a Mo(001) support induces site-specific nucleation of Cr and spatial ordering of Fe particles. The underlying modulations in the adsorption potential rely on several effects that control either the nucleation or the growth of the ad-metal. Individual Cr/Fe atoms preferentially bind to regions of high workfunction that enable electron transfer from the ad-species into the support. Particle growth, on the other hand, preferentially occurs in zones of contracted lattice parameter, where metal-metal and metal-oxide interactions can be optimized simultaneously. Both constraints favor particle growth in the Mg-Mo domains of the coincidence lattice. The observed ordering effect on the MgO thin films is therefore caused by interplay of geometric and electronic properties at the metal-oxide interface.

The MgO/Mo growth-template allows us to produce extended particle arrays with narrow size distribution. Owing to the high uniformity of the ensembles, distinct particle properties can thus be explored even with non-local spectroscopic techniques. This opens an experimentally simple route to address fundamental questions in heterogeneous catalysis, magnetism and nano-optics. As periodic modulations of structural and electronic properties are common for coincidence lattices in general, similar ordering phenomena are expected to occur for many other thin-film systems.

4. Experimental Section

The experiments were performed in two room-temperature STM setups operated at ultrahigh-vacuum conditions (2×10^{-10} mbar). The MgO films were prepared by reactive Mg-deposition in an O_2 ambience (5×10^{-7} mbar, 300 K), using a sputtered (1500 eV Ar^+) and annealed (2000 K) Mo(001) single-crystal support.[19] Film crystallization was achieved by annealing (1000 K) in vacuum. The film thickness was varied between 5 and 20 monolayers (ML), as derived from the attenuation of the Mo 3d lines in X-ray photoelectron spectroscopy. Low-energy-electron-diffraction data of the film displayed a square (1×1) pattern, indicative for a MgO(001) surface with the MgO[100] lattice vector being parallel to the Mo[110]. Reflex profiles were found to vary with film thickness and evolved from a central spot surrounded by four MgO[100]-oriented satellites (3-10 ML), to crossed-shaped (10-25 ML) and plain, circular reflexes (>25 ML).[21] These spot profiles indicate a certain film mosaicity, being induced by strain-compensation. Metal particles have been prepared by dosing Cr or Fe from an e-beam evaporator onto the freshly prepared films (0.5 ML min^{-1} atom-flux, 300 K). The nominal coverage was varied between 0.1 and 3 ML as calibrated with a quartz microbalance.

The nature of the MgO/Mo interface and its impact on the adsorption characteristic were analyzed by calculations performed on different levels of accuracy and complexity. Binding properties were determined with DFT calculations, using the generalized gradient exchange correlation functional by Perdew-Wang,[25] a plane-wave basis set (400 eV energy cut-off) and the projector augmented plane-wave method[26,27] as implemented in VASP.[28,29] The metal-oxide system was modelled with a slab comprising three MgO and five Mo layers separated by 10 Å of vacuum. A (2×2) and a (1×1) surface cell were used to calculate adatom and metal-bialyer binding energies, respectively. Dipole correction schemes were applied to eliminate electric fields perpendicular to the surface. The coordinates of adatoms and oxide ions as well as the vertical positions of the Mo species were relaxed until residual forces dropped below 0.01 eV $Å^{-1}$. Charges were evaluated with the Bader scheme.[30,31]

The influence of the MgO/Mo register on the Cr/Fe adsorption was evaluated with six model structures, in which the interface alignment was stepwise varied from Mg to O ions being on top of the Mo atoms. The in-plane lattice parameter was kept constant in these calculations in order to eliminate spurious effects due to changes of the Mo(001) workfunction. The role of substrate-induced distortions of the MgO lattice was evaluated independently with DFT calculations on unsupported, fully relaxed MgO trilayers having in-plane lattice parameters derived from our newly developed order-N approach.[22] In this semiempirical technique, the entire MgO/Mo superstructure can be described at once. Whereas the MgO trilayer is treated on the Hatree-Fock level, constraints due to the presence of the Mo(001) are accounted for by a potential energy surface fitted with results of our ab initio calculations.

Acknowledgements

S.B. and F.S. contributed equally to this work. The work was supported by the Italian MIUR through the FIRB Project RBAP115AYN "Oxides at the nanoscale: multifunctionality and applications" and the DFG excellence initiative "UNICAT". F.S. is grateful for a fellowship of the Humboldt foundation.

Received: June 5, 2012
Published online: August 13, 2012

[1] P. W. Murray, I. Brookes, S. A. Haycock, G. Thornton, *Phys. Rev. Lett.* **1998**, *80*, 988.
[2] M. P. Pileni, *J. Phys. Chem.* **2001**, *105*, 3358.
[3] A. Dmitriev, H. Spillmann, N. Lin, J. V. Barth, K. Kern, *Angew. Chem. Int. Ed.* **2003**, *42*, 2670.
[4] H. Brune, M. Giovannini, K. Bromann, K. Kern, *Nature* **1998**, *394*, 451.
[5] F. Leroy, G. Renaud, A. Letoublon, R. Lazzari, C. Mottet, J. Goniakowski, *Phys. Rev. Lett.* **2005**, *95*, 185501.
[6] N. Oncel, A. van Houselt, J. Huijben, A. S. Hallbäck, O. Gurlu, H. Zandvliet, B. Poelsema, *Phys. Rev. Lett.* **2005**, *95*, 116801.
[7] N. Nilius, E. Rienks, H.-P. Rust, H.-J. Freund, *Phys. Rev. Lett.* **2005**, *95*, 066101.
[8] P. Torelli, E. A. Soares, G. Renaud, L. Gragnaniello, S. Valeri, X. X. Guo, P. Luches, *Phys. Rev. B* **2008**, *77*, 081409.

[9] C. Becker, A. Rosenhahn, A. Wiltner, K. Bergmann, J. Schneider, P. Pervan, M. Milun, M. Kralj, K. Wandelt, *New J. Phys.* **2002**, *4*, 75.
[10] A. Mugarza, A. Mascaraque, V. Perez-Dieste, V. Repain, S. Rousset, F. J. Garcia de Abajo, J. E. Ortega, *Phys. Rev. Lett.* **2001**, *87*, 107601.
[11] N. Neel, J. Kröger, R. Berndt, *Appl. Phys. Lett.* **2006**, *88*, 163101.
[12] S. Ulrich, N. Nilius, H.-J. Freund, *Surf. Sci.* **2007**, *601*, 4603.
[13] M. Schmid, G. Kresse, A. Buchsbaum, E. Napetschnig, S. Gritschneder, M. Reichling, P. Varga, *Phys. Rev. Lett.* **2007**, *99*, 196104.
[14] L. Giordano, G. Pacchioni, J. Goniakowski, N. Nilius, E. D. L. Rienks, H.-J. Freund, *Phys. Rev. B* **2007**, *76*, 075416.
[15] F. Silly, M. Pivetta, M. Ternes, F. Patthey, J. Pelz, W. D. Schneider, *Phys. Rev. Lett.* **2004**, *92*, 016101.
[16] A. Sperl, J. Kroger, R. Berndt, *J. Phys. Chem. A* **2011**, *115*, 6973.
[17] X. Lin, N. Nilius, *J. Phys. Chem. C* **2008**, *112*, 15325.
[18] A. T. N'Diaye, S. Bleikamp, P. J. Feibelman, T. Michely, *Phys. Rev. Lett.* **2006**, *97*, 215501.
[19] S. Benedetti, H. M. Benia, N. Nilius, S. Valeri, H.-J. Freund, *Chem. Phys. Lett.* **2006**, *430*, 330.
[20] H. J. Freund, G. Pacchioni, *Chem. Soc. Rev.* **2008**, *37*, 2224.
[21] S. Benedetti, P. Torelli, S. Valeri, H. M. Benia, N. Nilius, G. Renaud, *Phys. Rev. B* **2008**, *78*, 195411.
[22] C. Noguera, J. Godet, J. Goniakowski, *Phys. Rev. B* **2010**, *81*, 155409.
[23] H. M. Benia, P. Myrach, N. Nilius, H.-J. Freund, *Surf. Sci.* **2010**, *604*, 435.
[24] H. M. Benia, P. Myrach, A. Gonchar, T. Risse, N. Nilius, H.-J. Freund, *Phys. Rev. B* **2010**, *81*, 241415(R).
[25] J. P. Perdew, J. A. Chevary, S. H. Vosko, K. A. Jackson, M. R. Pederson, D. J. Singh, C. Fiolhais, *Phys. Rev. B* **1992**, *46*, 6671.
[26] P. E. Blöchl, *Phys Rev. B* **1994**, *50*, 17953.
[27] O. Bengone, M. Alouani, P. E. Blöchl, J. Hugel, *Phys Rev. B* **2000**, *62*, 16392.
[28] G. Kresse, J. Hafner, *Phys Rev. B* **1993**, *47*, R558.
[29] G. Kresse, J. Furthmüller, *Phys. Rev. B* **1996**, *54*, 11169.
[30] R. F. W. Bader, *Chem Rev.* **1991**, *91*, 983.
[31] a) G. Henkelman, A. Arnaldsson, H. Jónsson, *Comput. Mater. Sci.* **2006**, *36*, 254; b) W. Tang, E. Sanville, G. Henkelman, *J. Phys.: Condens. Matter* **2009**, *21*, 084204.